DRDC-RDDC-2016-P104

Mid-infrared nonlinear absorption in As_2S_3 chalcogenide glass

Francis Théberge,[1,*] Pierre Mathieu,[1] Nicolas Thiré,[2] Jean-François Daigle,[1] Bruno E. Schmidt,[2,3] Jean Fortin,[1] Réal Vallée,[4] Younès Messaddeq,[4] and François Légaré[2]

[1]*Defence R&D Canada Valcartier, 2459 de la Bravoure Blvd, Québec (Qc), G3J 1X5, Canada*
[2]*INRS-EMT, 1650 Lionel-Boulet Blvd, Varennes (Qc), J3X 1S2, Canada*
[3]*Few-Cycle Inc., 2890 de Beaurivage Street, Montréal (Qc), H1L 5W5, Canada*
[4]*Center for Optics, Photonics, and Lasers (COPL), Université Laval, Québec G1V 0A6, Canada*
[*]*francis.theberge@drdc-rddc.gc.ca*

Abstract: We report mid-infrared (MIR) nonlinear absorption in As_2S_3 glasses which results from two-photon excitation of valence electron to the Urbach extension followed by strong linear absorption of excited states. The measured MIR nonlinear absorption can be 3 to 4 orders of magnitude stronger than the two-photon absorption in the near-infrared for similar laser intensities and does not result from contaminants, but it is intrinsic to As_2S_3 glasses. As_2S_3 fibers are widely used to generate supercontinuum by pumping them with high peak power laser pulses. For a 100 kilowatt peak power MIR soliton propagating in single mode As_2S_3 fiber, the nonlinear absorption can be of similar magnitude than the fiber background loss. Finally, for laser peak power around 1 MW, the MIR nonlinear absorption can be ~2 orders of magnitude larger than the fiber background loss in single mode As_2S_3 fiber.

OCIS codes: (190.4370) Nonlinear optics, fibers; (060.2390) Fiber optics, infrared; (320.6629) Supercontinuum generation.

References and links

1. M. El-Amraoui, J. Fatome, J. C. Jules, B. Kibler, G. Gadret, C. Fortier, F. Smektala, I. Skripatchev, C. F. Polacchini, Y. Messaddeq, J. Troles, L. Brilland, M. Szpulak, and G. Renversez, "Strong infrared spectral broadening in low-loss As-S chalcogenide suspended core microstructured optical fibers," Opt. Express **18**(5), 4547–4556 (2010).
2. A. Marandi, C. W. Rudy, V. G. Plotnichenko, E. M. Dianov, K. L. Vodopyanov, and R. L. Byer, "Mid-infrared supercontinuum generation in tapered chalcogenide fiber for producing octave-spanning frequency comb around 3 μm," Opt. Express **20**(22), 24218–24225 (2012).
3. R. R. Gattass, L. B. Shaw, V. Q. Nguyen, P. C. Pureza, I. D. Aggarwal, and J. S. Sanghera, "All-fiber chalcogenide-based mid-infrared supercontinuum source," Opt. Fiber Technol. **18**(5), 345–348 (2012).
4. J. Hu, C. R. Menyuk, L. B. Shaw, J. S. Sanghera, and I. D. Aggarwal, "A mid-IR source with increased bandwidth using tapered As_2S_3 chalcogenide photonic crystal fibers," Opt. Commun. **293**, 116–118 (2013).
5. W. Gao, M. El Amraoui, M. Liao, H. Kawashima, Z. Duan, D. Deng, T. Cheng, T. Suzuki, Y. Messaddeq, and Y. Ohishi, "Mid-infrared supercontinuum generation in a suspended-core As_2S_3 chalcogenide microstructured optical fiber," Opt. Express **21**(8), 9573–9583 (2013).
6. O. Mouawad, J. Picot-Clémente, F. Amrani, C. Strutynski, J. Fatome, B. Kibler, F. Désévédavy, G. Gadret, J.-C. Jules, D. Deng, Y. Ohishi, and F. Smektala, "Multioctave midinfrared supercontinuum generation in suspended-core chalcogenide fibers," Opt. Lett. **39**(9), 2684–2687 (2014).
7. J. S. Sanghera, I. D. Aggarwal, L. B. Shaw, C. M. Florea, P. Pureza, V. Q. Nguyen, F. Kung, and I. D. Aggarwal, "Nonlinear properties of chalcogenide glass fibers," J. Optoelectron. Adv. Mater. **8**, 2148–2155 (2006).
8. J. Troles, Q. Coulombier, G. Canat, M. Duhant, W. Renard, P. Toupin, L. Calvez, G. Renversez, F. Smektala, M. El Amraoui, J. L. Adam, T. Chartier, D. Mechin, and L. Brilland, "Low loss microstructured chalcogenide fibers for large non linear effects at 1995 nm," Opt. Express **18**(25), 26647–26654 (2010).
9. C. Xiong, E. Magi, F. Luan, A. Tuniz, S. Dekker, J. S. Sanghera, L. B. Shaw, I. D. Aggarwal, and B. J. Eggleton, "Characterization of picosecond pulse nonlinear propagation in chalcogenide As(2)S(3) fiber," Appl. Opt. **48**(29), 5467–5474 (2009).
10. R. Cherif and M. Zghal, "Ultrabroadband, midinfrared supercontinuum generation in dispersion engineered As_2Se_3-based chalcogenide photonic crystal fibers," Int. J. Opt. **2013**, 1–6 (2013).
11. D. D. Hudson, S. A. Dekker, E. C. Mägi, A. C. Judge, S. D. Jackson, E. Li, J. S. Sanghera, L. B. Shaw, I. D. Aggarwal, and B. J. Eggleton, "Octave spanning supercontinuum in an As_2S_3 taper using ultralow pump pulse energy," Opt. Lett. **36**(7), 1122–1124 (2011).

12. K. F. Lee, N. Granzow, M. A. Schmidt, W. Chang, L. Wang, Q. Coulombier, J. Troles, N. Leindecker, K. L. Vodopyanov, P. G. Schunemann, M. E. Fermann, P. St. J. Russell, and I. Hartl, "Midinfrared frequency combs from coherent supercontinuum in chalcogenide and optical parametric oscillation," Opt. Lett. **39**(7), 2056–2059 (2014).
13. F. Théberge, N. Thiré, J.-F. Daigle, P. Mathieu, B. E. Schmidt, Y. Messaddeq, R. Vallée, and F. Légaré, "Multioctave infrared supercontinuum generation in large-core As_2S_3 fibers," Opt. Lett. **39**(22), 6474–6477 (2014).
14. C. R. Petersen, U. Møller, I. Kubat, B. Zhou, S. Dupont, J. Ramsay, T. Benson, S. Sujecki, N. Abdel-Moneim, Z. Tang, D. Furniss, A. Seddon, and O. Bang, "Mid-infrared supercontinuum covering the 1.4–13.3 μm molecular fingerprint region using ultra-high NA chalcogenide step-index fibre," Nat. Photonics **8**(11), 830–834 (2014).
15. Y. Yu, B. Zhang, X. Gai, C. Zhai, S. Qi, W. Guo, Z. Yang, R. Wang, D.-Y. Choi, S. Madden, and B. Luther-Davies, "1.8-10 μm mid-infrared supercontinuum generated in a step-index chalcogenide fiber using low peak pump power," Opt. Lett. **40**(6), 1081–1084 (2015).
16. Y. Yu, X. Gai, T. Wang, P. Ma, R. Wang, Z. Yang, D.-Y. Choi, S. Madden, and B. Luther-Davies, "Mid-infrared supercontinuum generation in chalcogenides," Opt. Mater. Express **3**(8), 1075–1086 (2013).
17. O. Mouawad, P. Béjot, F. Billard, P. Mathey, B. Kibler, F. Désévédavy, G. Gadret, J.-C. Jules, O. Faucher, and F. Smektala, "Mid-infrared filamentation-induced supercontinuum in As-S and As-free Ge-S counterpart chalcogenide glasses," Appl. Phys. B **121**(4), 433–438 (2015).
18. M. Asobe, K. Suzuki, T. Kanamori, and K. Kubodera, "Nonlinear refractive index measurement in chalcogenide-glass fibers by self-phase modulation," Appl. Phys. Lett. **60**(10), 1153 (1992).
19. D. C. Hutchings, M. Sheik-Bahae, D. J. Hagan, and E. W. Van Stryland, "Kramers-Krönig relations in nonlinear optics," Opt. Quantum Electron. **24**(1), 1–30 (1992).
20. K. Tanaka, "Two-photon absorption spectroscopy of As_2S_3 glass," Appl. Phys. Lett. **80**(2), 177–179 (2002).
21. S. Dai, F. Chen, Y. Xu, Z. Xu, X. Shen, T. Xu, R. Wang, and W. Ji, "Mid-infrared optical nonlinearities of chalcogenide glasses in Ge-Sb-Se ternary system," Opt. Express **23**(2), 1300–1307 (2015).
22. M. Sheik-Bahae, A. A. Said, T. H. Wei, D. J. Hagan, and E. W. Van Stryland, "Sensitive measurement of optical nonlinearities using a single beam," IEEE J. Quantum Electron. **26**(4), 760–769 (1990).
23. M. Sheik-Bahae, A. A. Said, D. J. Hagan, M. J. Solieau, and E. W. Van Stryland, "Nonlinear refraction and optical limiting in thick media," Opt. Eng. **30**, 1228–1235 (1991).
24. F. Gholami, S. Zlatanovic, A. Simic, L. Liu, D. Borlaug, N. Alic, M. Nezhad, Y. Fainman, and S. Radic, "Third order nonlinearity in silicon beyond 2350 nm," Appl. Phys. Lett. **99**(8), 081102 (2011).
25. A. D. Bristow, N. Rotenberg, and H. M. van Driel, "Two-photon absorption and Kerr coefficients of silicon for *850-2200 nm*," Appl. Phys. Lett. **90**(19), 191104 (2007).
26. N. Venkatram, R. Sathyavathi, and D. N. Rao, "Size dependent multiphoton absorption and refraction of CdSe *nanoparticles*," Opt. Express **15**(19), 12258–12263 (2007).
27. B. E. Schmidt, A. D. Shiner, M. Giguère, P. Lassonde, C. A. Trallero-Herrero, J.-C. Kieffer, P. B. Corkum, D. M. Villeneuve, and F. Légaré, "High harmonic generation with long-wavelength few-cycle laser pulses," J. Phys. At. Mol. Opt. Phys. **45**(7), 074008 (2012).
28. Q. Lin, J. Zhang, G. Piredda, R. W. Boyd, P. M. Fauchet, and G. P. Agrawal, "Dispersion of silicon nonlinearities in the near infrared region," Appl. Phys. Lett. **91**(2), 021111 (2007).
29. T. Wang, N. Venkatram, J. Gosciniak, Y. Cui, G. Qian, W. Ji, and D. T. H. Tan, "Multi-photon absorption and third-order nonlinearity in silicon at mid-infrared wavelengths," Opt. Express **21**(26), 32192–32198 (2013).
30. X. Gai, Y. Yu, B. Kuyken, P. Ma, S. J. Madden, J. Van Campenhout, P. Verheyen, G. Roelkens, R. Baets, and B. Luther-Davies, "Nonlinear absorption and refraction in crystalline silicon in the mid-infrared," Laser Photonics Rev. **7**(6), 1054–1064 (2013).
31. M. F. Churbanov, I. V. Scripatchev, G. E. Snopatin, V. S. Shiryaev, and V. G. Plotnichenko, "High purity glasses based on arsenic chalcogenides," J. Optoelectron. Adv. Mater. **3**, 341–349 (2001).
32. M. Bass, E. W. Van Stryland, D. R. Williams, and W. L. Wolfe, *Handbook of Optics* (McGraw-Hill, 1995), Ch. 33.
33. V. Verlan, "Density of localized state of free carriers in amorphous As_2Se_3 and As_2S_3 films," IEEE Semiconductor Conf. **2**, 423–426 (2002).
34. R. L. Sutherland, M. C. Brant, J. Heinrichs, J. E. Rogers, J. E. Slagle, D. G. McLean, and P. A. Fleitz, "Excited-state characterization and effective three-photon absorption model of two-photon-induced excited-state absorption in organic push-pull charge-transfer chromophores," J. Opt. Soc. Am. B **22**(9), 1939–1948 (2005).
35. B. Gu, W. Ji, P. S. Patil, S. M. Dharmaprakash, and H.-T. Wang, "Two-photon-induced excited-state absorption: Theory and experiment," Appl. Phys. Lett. **92**(9), 091118 (2008).
36. D. von der Linde and H. Schuler, "Breakdown threshold and plasma formation in femtosecond laser–solid interaction," J. Opt. Soc. Am. B **13**(1), 216–222 (1996).
37. C. Schaffer, N. Nishimura, E. Glezer, A. Kim, and E. Mazur, "Dynamics of femtosecond laser-induced breakdown in water from femtoseconds to microseconds," Opt. Express **10**(3), 196–203 (2002).
38. M. Durand, A. Houard, K. Lim, A. Durécu, O. Vasseur, and M. Richardson, "Study of filamentation threshold in zinc selenide," Opt. Express **22**(5), 5852–5858 (2014).
39. L. Ren, B. Yao, X. Hou, L. Liu, and C. Zhou, "Analyses and computations of asymmetric Z-scan for large phase shift from diffraction theory," Chin. Opt. Lett. **1**, 111–113 (2003).

40. S.-Q. Chen, Z.-B. Liu, W.-P. Zang, J.-G. Tian, W.-Y. Zhou, F. Song, and C.-P. Zhang, "Study on Z-scan charateristics for a large nonlinear phase shift," J. Opt. Soc. Am. B **22**(9), 1911–1916 (2005).
41. H. Schroeder and S. L. Chin, "Visualization of the evolution of multiple filaments in methanol," Opt. Commun. **234**(1-6), 399–406 (2004).
42. S. L. Chin, S. A. Hosseini, W. Liu, Q. Luo, F. Théberge, N. Aközbek, A. Becker, V. P. Kandidov, O. G. Kosareva, and H. Schroeder, "The propagation of powerful femtosecond laser pulses in optical media: physics, applications, and new challenges," Can. J. Phys. **83**(9), 863–905 (2005).

1. Introduction

Supercontinuum (SC) generation in chalcogenide fiber is widely tested in order to generate broadband spectrum spanning from visible up to the far-infrared [1–6]. The chalcogenide fibers are very promising because of their wide transmission window. The As_2S_3 based fiber can transmit from 700 nm up to ~7 μm and the As_2Se_3 can transmit from 1 μm to ~9 μm [7,8]. SC generation requires powerful laser pulse and Erbium-doped fiber and Thulium-doped fiber based near-infrared (NIR) lasers are efficient and commercially available. However in order to minimize the nonlinear absorption (NLA) in chalcogenide fiber when pumped with NIR lasers, it is commonly expected that As_2S_3 fibers are preferable as compared to the As_2Se_3 because of its wider bandgap [9]. Also the zero dispersion wavelength (ZDW) of As_2Se_3 is around 5.5 μm while that of As_2S_3 is around 4.5 μm [1,10], which is closer to the pump wavelength of commercial lasers. In order to generate broadband SC in As_2S_3 fiber, the main technique uses microstrutured fibers in order to shift the dispersion of the fiber close to the laser pump wavelengths [1,5]. With such technique, the core of the As_2S_3 microstrutured fiber is reduced to 3-5 μm. Similarly, the fabrication of tapered As_2S_3 fiber [2,4,11,12] with core diameter reduced to 2-3 μm was used also to increase the laser intensity in the fiber core over a short distance in order to enhance the spectral broadening through nonlinear intensity dependent effects as self-phase modulation and self-frequency shift Raman soliton. However, with all these techniques, the broadest reported 20 dB spectral bandwidth SC spans only over ~3000 nm, and none of them was shown to extend beyond 4.2-4.5 μm. This limitation was attributed to the S-H absorption band centered at 4.2 μm, which is a common contaminant in As_2S_3 fiber. During the continuous red-shift of the Raman soliton, the Raman shift cannot jump over the S-H absorption band at 4.2 μm [3], consequently, the SC expansion in the fiber was blocked by this absorption band. A lot of effort has been made to produce high purity As_2S_3 fiber with very low S-H contamination. Such improvements of the chalcogenide transmissions and its inherent high nonlinear response allowed the generation of ultrabroadband SC in chalcogenide fibers [13–15] or even in chalcogenide bulk glasses [16,17] by using mid-infrared ultrashort laser pulses from solid-state laser systems. Intensities of pump laser pulses injected in these chalcogenide fibers or glass samples were high, from 10 GW/cm^2 to 1 TW/cm^2 [13–17], and SC generation was covering the complete transmission of chalcogenide materials.

The magnitude of As_2S_3 nonlinear index of refraction is large [7,18] as compared to fluoride glasses and through the Kramer-Kröning relation [19], we can expect that chalcogenide glasses possess also a relatively high NLA. Previous measurement of the NLA in As_2S_3 and As_2Se_3 are limited in the near infrared, usually for wavelength below 2.5 μm [20,21].

In this paper we measured the mid-infrared (MIR) nonlinear absorption in As_2S_3 glasses. Usually, for multi-photon absorption, it is expected that the NLA is lower for lower energy photons (longer wavelength) because it is a higher order nonlinear effect. However, we demonstrate in this paper that the NLA between 3.9 and 4.5 μm can be 3-4 orders of magnitude stronger than the two-photon absorption in the NIR. The stronger NLA in the MIR is not due to contaminants in As_2S_3 glasses, but is intrinsic to the As_2S_3 molecules and results from two-photon absorption followed by strong linear absorption of excited-states. Depending of the MIR laser intensity injected into the fiber, the NLA can be much higher than the fiber

background loss. These results are important for optimizing the average output power of broadband supercontinuum source produced through nonlinear propagation in As_2S_3 fibers.

2. Experimental setup

Nonlinear absorption in As_2S_3 was measured in the NIR and MIR using the Z-scan technique [22–26]. Z-scan has been widely adopted as a convenient technique using single beam to obtain multi-photon absorption coefficients and nonlinear refractive index with the position-dependent transmittance variation by scanning a sample through the focal region of a Gaussian laser beam (see Fig. 1(a)). These experiments were performed using the infrared beam line at the Advanced Laser Light Source (ALLS) [27]. In a first step, we used 70 fs pulses (pulsewidth measured by frequency resolved optical gating) at 2 μm from an optical parametric amplifier pumped by 800 nm Ti:Sapphire regenerative amplifier at 100 Hz. Secondly, with a difference frequency generation crystal, it was possible to produce ultrashort MIR laser pulses that were spectrally narrowed with a bandpass filter centered either at 3.9 μm or 4.56 μm, which correspond to wavelengths below and above the S-H contaminant absorption band of As_2S_3, respectively. The pulsewidth at both wavelengths was 130 fs and the laser pulses were focused at normal incidence angle onto samples using a 10 cm long CaF_2 focal length lens. The diameter of the incident laser beams were 4 mm at full width at half maximum for the three laser wavelengths used. Due to potential irregularities and asymmetries from input beam profiles, laser beam diameters were measured along the scanned axis in order to quantify precisely the laser intensity distribution for each position along the z-axis. The transmitted optical signal was collected by another CaF_2 lens with 5 cm focal length and focused onto a PbSe photoconductive detector sensitive in the range of wavelength between 1 μm and 4.8 μm. The effective NLA were extracted from open-aperture Z-scan measurements [22,23].

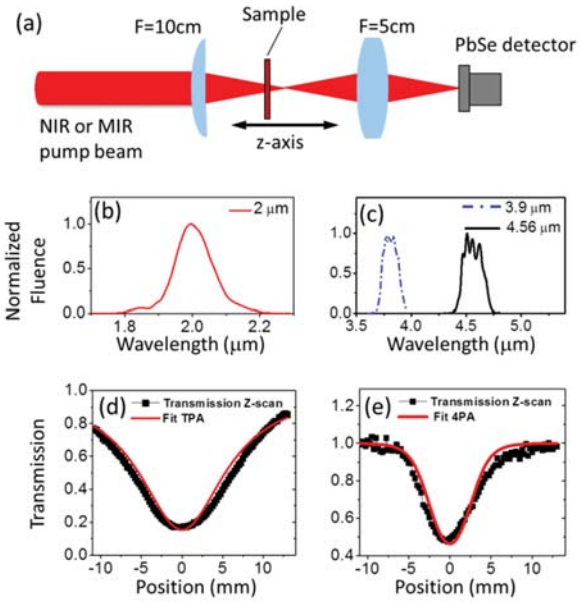

Fig. 1. (a) Z-scan setup. (b) Spectral distribution for the NIR pump pulse. (c) Spectral distribution for the MIR pump pulses. (d) Z-scan trace in silicon and two-photon absorption (TPA) fit at 2 μm pump wavelength. (e) Z-scan trace in silicon and four-photon absorption (4PA) fit at 4.56 μm pump wavelength.

Before doing z-scan experiment on As_2S_3 samples, we first performed Z-scan experiments on 0.5 mm thick silicon sample to verify the calibration of our setup. NLA of silicon is well documented in the NIR because of its wide applications in integrated photonics. Figure 1(d) presents the measured transmission of the 2 μm femtosecond laser as a function of the silicon sample position along the Z-axis. These experimental results can be well fitted with the multi-photon transmission model given by [22–25]:

$$T = \left[\sqrt[n-1]{\left(1 + d\,(n+1)\,\alpha_n I^{n-1}(z)\right)} \right]^{-1}. \quad (1)$$

Here T is the transmission, I is the pump intensity, d is the sample thickness, n is the multi-photon order and α_n is the n-photon NLA parameter. For the 2 μm pump wavelength, the best fit for the silicon sample was achieved with the two-photon absorption (TPA) fit presented in Fig. 1(d), and the parameters were $n = 2$ and $\alpha_2 = 0.075 \pm 0.02$ cm/GW . This TPA parameter for silicon corresponds very well to previously published results [25,28]. Figure 1(e) presents the Z-scan of the silicon sample when using the 4.56 μm femtosecond laser. For this pump wavelength, the best fit for the silicon sample was achieved with the four-photon absorption (4PA) fit presented in Fig. 1(e), and the parameters were $n = 4$ and $\alpha_4 = 5 \pm 2\text{E-}7\ \text{cm}^5/\text{GW}^3$ [29]. It is important to note that free carrier absorption (FCA) in silicon was negligible for the laser parameters used for these tests. According to the FCA cross-section measured in [30], the transmission loss induced by FCA during the 4.56 μm laser Z-scan was calculated to be <0.6%, which is negligible as compared to the multi-photon absorption observed in Fig. 1(e). The slight asymmetry of the Z-scan curve in Fig. 1(e) is due to irregularities and asymmetries from the input laser beam profile. This was confirmed by observing slight deviations of Z-scan measurements relative to Z-scan fits (using perfect Gaussian beam profile) at same z-axis positions for different laser intensities, different samples, and different sample thicknesses. However, precise measurements of the NLA as a function of laser intensity were obtained because the laser beam distributions were measured for each position along the z-axis.

3. Results

The linear absorption of the As_2S_3 samples tested for the NLA measurement is presented in Fig. 2(a). The sample A was purified and produced at Laval University and the dimension of the window was 25 mm diameter by 2.4 mm thick. This sample was very pure and no contaminants were detected through infrared spectroscopy, with a detection limit for S-H group smaller than 0.3 ppm. A 2.9 mm thick glass sample B was also made of As_2S_3 but contaminated with H_2O, S-H and –OH groups. The concentration of S-H in sample B was around 50 ppm [31]. Example of z-scan measurement for As_2S_3 samples are given in Fig. 2(b) for pump wavelength at 4.56 μm. This pump wavelength is around the zero dispersion wavelength of As_2S_3 and since high pump intensities were used, we verified if important spectral broadening occurred when the pump laser was focused in As_2S_3 samples [16]. Figure 2(c) presents the output spectrum of the 4.56 μm pump laser when the As_2S_3 sample is positioned at the focus (z = 0 mm), at 3 mm and 13 mm after the focus. Nevertheless the high pump intensities used, these samples were thin enough to avoid spectral broadening, as confirmed in Fig. 2(c).

For the measurement of the NLA in As_2S_3, a Fresnel reflection loss of 17% for the first As_2S_3 surface was measured for the three laser wavelengths used. Figure 3 presents the measured effective NLA expressed in dB/m in order to better compare it with the linear absorption shown in Fig. 2(a). At 2 μm pump wavelength, the NLA in As_2S_3 samples could be

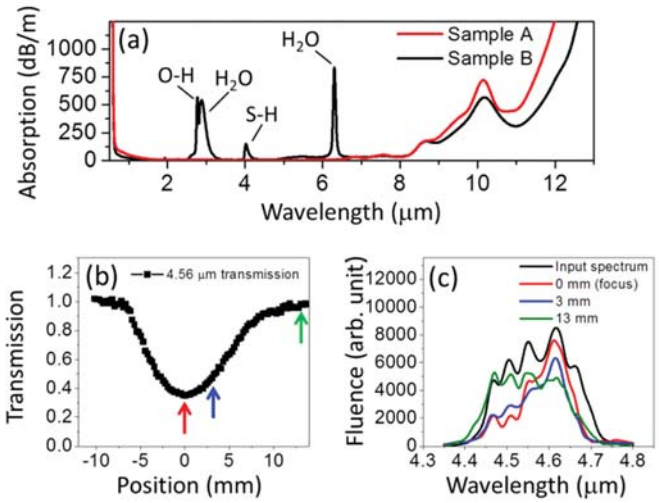

Fig. 2. (a) Linear absorption spectrum of two As_2S_3 chalcogenide samples. (b) Z-scan trace in As_2S_3 sample A at 4.56 μm pump wavelength. Arrows indicate the positions where the output spectrum of the pump laser was measured. (c) Spectral distribution for the output 4.56 μm pump pulses for different position of the As_2S_3 sample along the Z-axis.

detected starting at a laser intensity of 40 GW/cm^2. These experimental results could be well fitted with the multi-photon absorption model where the nonlinear loss (L_{nl}) expressed in dB/m is given by [22,23]:

$$L_{nl} = -10\log\left\{\exp\left(\frac{-\ln\left(\left[1+(n-1)\alpha_n I^{n-1} d\right]^{1/(n-1)}\right)}{d}\right)\right\}. \qquad (2)$$

For the 2 μm pump wavelength, the best fit was achieved with the two-photon absorption (TPA) fit presented in Fig. 3, and the parameters were $n = 2$ and $\alpha_2 \cong 0.0014$ cm/GW for both As_2S_3 samples A and B. This TPA value of As_2S_3 corresponds very well to previously published results [20].

An unexpectedly stronger NLA - than for the shorter 2.0 μm pump wavelength- was observed for both the 3.9 μm and 4.56 μm wavelengths. The NLA in this range of wavelengths has not been reported before for As_2S_3. At 3.9 μm and 4.56 μm pump wavelengths, the NLA in As_2S_3 samples could be detected starting at laser intensities around 40 GW/cm^2 for a pulsewidth of 130 fs. For laser intensity above 50 GW/cm^2, the MIR NLA becomes more important than at 2 μm pump wavelength. Also, in opposite to the 2 μm pump wavelength, we observed a saturation of the nonlinear loss at higher laser intensities for the 3.9 and 4.56 μm wavelengths. These experimental results using MIR pump pulses could not be well fitted with the multi-photon absorption model expressed in Eqs. (1) and (2). There were divergences between the multi-photon absorption fit and the experimental results either at low or high laser intensities depending of the fit parameters used. In particular, the multi-photon absorption model cannot reproduce the saturation of the MIR NLA observed at higher laser intensities. Therefore another model must be developed in order to clarify the measured experimental results.

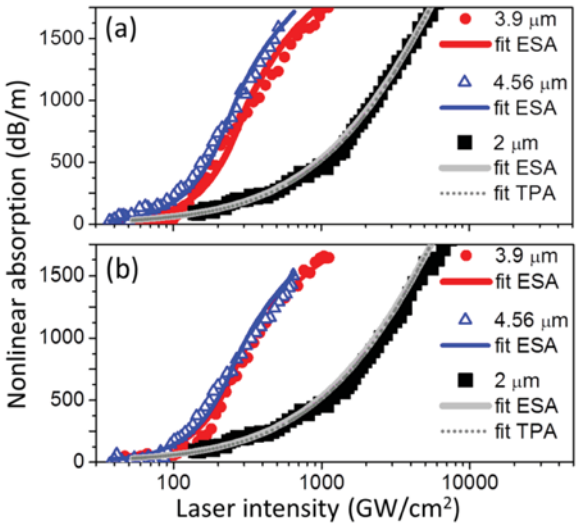

Fig. 3. Measured and simulated nonlinear absorption as a function of laser intensity for different pump wavelengths. (a) For sample A made of pure As_2S_3, and (b) for sample B with contaminated As_2S_3.

4. Analysis

Figure 4 presents the schematic representation of the energy level in As_2S_3, which have a bandgap of 2.3 eV. In the case of amorphous materials such as chalcogenide glass, an exponential Urbach extension [32,33] exists and its absorption edge extends below the half gap. The grey zone between the conduction band and the valence band in Fig. 4 represents this Urbach extension for which the lowest energy level measured is less than 0.6-0.7 eV above the valence band [33]. Under irradiation of 0.6 eV photon (wavelength of 2 μm), single photon excitation from the valence band to the Urbach extension can occur (represented by $h\nu_{NIR}$ in Fig. 4). For high photon flux, the excited electron in the Urbach extension can be either excited at a higher energy level in the Urbach extension or de-excited to the valence band through stimulated emission. However, the stimulated emission from 2 μm decrease the electron population in the Urbach extension and limit therefore the absorption of 0.6 eV photons (wavelength of 2 μm) at upper levels in the Urbach extension. For 2 μm wavelength, this process corresponds to excited state absorption (ESA), which has similar intensity dependence than two-photon absorption. For lower photon energy (longer wavelength), multi-photon absorption must occur to excite valence electron to the Urbach extension. For wavelength around 3.9 μm and 4.56 μm (photon energy around 0.3 eV), two-photon absorption is required to excite the electron to the Urbach extension (represented by $h\nu_{MIR}$ in Fig. 4). Contrarily to photon with twice the energy, the 0.3 eV photon cannot de-excite the Urbach electron to the valence band through stimulated emission. Therefore, once valence electrons are excited to the Urbach extension by MIR two-photon absorption, the Urbach extension is rapidly populated by these electrons which are trapped for an extended time, usually a lifetime of ns time scale [34,35], which is much longer than the 70-130 fs pulsewidth used in these experiments. These Urbach electrons can further absorb single MIR photon and progress upward in the energy diagram up to the conduction band through MIR linear absorption. This process corresponds also to ESA, but this time it will be similar to two-photon absorption followed by strong linear absorption from excited states.

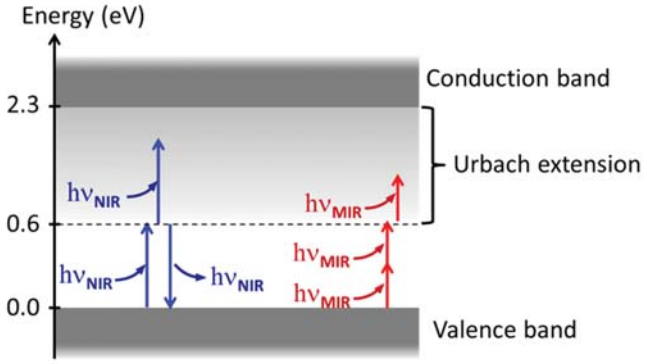

Fig. 4. Schematic representation of energy diagram of As_2S_3 and the multi-photon excitation processes.

A better representation of these observed NLA can be obtained with the nonlinear excited state absorption model [34,35]. Here the lifetime of the excited electron in the Urbach extension is in the nanosecond time scale and therefore the spontaneous de-excitation can be neglected in comparison with the laser pump pulsewidths used in our experiment. Therefore, by neglecting the spontaneous de-excitation, the nonlinear excited state absorption can be simulated by numerically integrating the following set of equations:

$$\frac{\partial I}{\partial z} = -\sigma_n N_0 I^n - \sigma_s N_s I \tag{3}$$

$$N_s(t) = \frac{\sigma_n N_0}{n h\nu} \int_{-\infty}^{t} I^n(t')\, dt' \tag{4}$$

$$N_0(t) = N - N_s(t) \tag{5}$$

Here $I(z,t)$ is the laser intensity distribution, $N = 7.759\text{E}21$ cm^{-3} is the molecular density of As_2S_3, N_0 and N_S are the molecular density in the valence band and in the excited states, respectively. σ_n and σ_S are the NLA cross section and the effective excited state absorption cross section, $h\nu$ is the photon energy and n is the number of photon absorbed to reach an excited state in the Urbach extension. These equations were numerically integrated in time and over the thickness of the As_2S_3 sample by assuming an initial spatial and temporal Gaussian distribution for the laser intensity and by assuming $N_0(t = -\infty) = N$.

The best parameter values for the nonlinear excited state absorption fits presented in Fig. 3 are given in Tables 1 and 2. For the 2 μm pump wavelength, we obtained with the excited state absorption model the same fit than with Eq. (2). However, at laser intensities above 300 GW/cm^2 for pump wavelength at 3.9 μm and 4.56 μm, we observed a saturation of the NLA for both the experimental and numerical data, which could not be represented with Eq. (2). This saturation results from the electron depopulation of the valence band toward the Urbach extension by the high intensity leading edge of the laser pulse. Consequently, the two-photon absorption is reduced due to the depopulation of the valence band and mainly single photon absorption occurs in the Urbach extension for the backward part of the laser pulse, which results in a damped NLA for input laser intensities higher than 300 GW/cm^2. It is important to note that femtosecond laser pulse excitation of electrons in glasses is mainly governed by multi-photon excitation. Avalanche excitation is limited because the electrons are not accelerated enough during the short laser pulsewidth. Therefore, at the intensities and pulsewidths used in our experiments, optical breakdown does not occur [36–38].

Table 1. Nonlinear absorption parameters for sample A

Wavelength	2 µm	3.9 µm	4.56 µm
n	1	2	2
σ_n	2.0 ± 0.3 E –25 cm^2	2.1 ± 0.3 E –26 cm^4/GW	2.6 ± 0.5 E –26 cm^4/GW
$\sigma_S\left(cm^2\right)$	6.5 ± 0.7 E –22	6.3 ± 0.4 E –22	6.5 ± 0.4 E –22

Table 2. Nonlinear absorption parameters for sample B

Wavelength	2 µm	3.9 µm	4.56 µm
n	1	2	2
σ_n	2.0 ± 0.3 E –25 cm^2	2.5 ± 0.3 E –26 cm^4/GW	2.3 ± 0.5 E –26 cm^4/GW
$\sigma_S\left(cm^2\right)$	6.5 ± 0.7 E –22	5.6 ± 0.3 E –22	5.9 ± 0.3 E –22

When comparing the NLA cross section and the ESA cross section for the samples A and B, we notice very similar parameters which point out the negligible impact of contaminant in the measured MIR NLA. The observed MIR NLA is intrinsic to the As_2S_3 glasses and is the direct consequence of the existence of an Urbach extension.

According to the density level of the Urbach extension in As_2S_3 [33], this MIR NLA corresponds to two-photon absorption followed by linear absorption from excited states. Such two-photon absorption should begin for wavelength above 3 µm (photon energy < 0.4 eV) and below 5 µm (photon energy > 0.25 eV). For pump wavelength longer than 5 µm, a three-photon absorption is required to excite electrons to the Urbach extension and such NLA should be less important than the NLA measured around 3.9 µm and 4.56 µm for the range of laser intensities explored in this paper.

Z-scan technique is a precise method based on self-focusing to measure the nonlinear optical response of materials. For the highest laser intensities presented in this paper and according to sample thicknesses used, large nonlinear phase shifts were accumulated by the probe laser pulses during the Z-scan. It has been demonstrated in [39,40] that nonlinear refractive index measurements can be done for large nonlinear phase shift and NLA measurements are not affected by such large phase shift. In our measurements, self-focusing could have generated multiple hot-spots across the laser beam profile which were initiated by intensity irregularities across the laser beam profile [41,42]. Each hot-spot could increase locally the laser intensity, but decreased the laser intensity between these hot-spots. Such multiple hot-spots self-focusing could induce some errors on the effective intensity. However, the NLA measurements presented in this paper for silicon at 2 µm and 4.56 µm corresponded to previously published results by three different groups [25,28,29]. Moreover, the nonlinear absorption in As_2S_3 at 2 µm was equivalent to previously published results [20]. These corroborations with previously published results indicate that self-focusing into samples produced minor or even negligible errors on the effective intensity during the Z-scan.

To further confirm these results, ultrashort and intense 4.56 µm laser pulses were injected in large core As_2S_3 fibers in order to measure their output energy and generated supercontinuum for different fiber length. The As_2S_3 chalcogenide fiber used has been produced at CorActive (product IRT-SU-100/170) and the transmission loss of this 100 µm core fiber is presented in Fig. 5(a). This high purity As_2S_3 fibers exhibit a MIR background loss of 0.2 dB/m and a loss inferior to 0.55 dB/m at the S-H absorption peak around 4.05 µm. For these tests, both fiber ends were cleaved by a diamond stylus to ensure a sufficiently flat interface. The generated and transmitted supercontinuum was measured by an f = 12.5 cm monochromator purged with dry nitrogen and equipped with a 300 lines/mm diffraction grating providing a spectral resolution around 5 nm. A PbSe detector was used to measure the spectral fluence for wavelength range between 1 µm and 4.8 µm, and a liquid nitrogen cooled HgCdTe detector from 2 µm to 13 µm. In order to block any higher diffraction order of the

grating overlapping with the supercontinuum spectrum, a Germanium window was used in front of the detectors to record the spectrum between 1.9 µm up to 3.5 µm. To record the spectrum between 3 µm up to 5.5 µm, a long pass filter transmitting above 3 µm was used and to record the spectrum between 4.5 µm up to 9 µm, a long pass filter transmitting above 4.5 µm was used. The complete spectral distribution was reconstructed by combining the overlapping spectra from each combination of detector and long pass filter. Figures 5(b)-5(f) presents the supercontinuum evolution as a function of the fiber length. The energy injected into the core of the fiber was 700 nJ. Most of the spectral broadening occurred in the first centimeters of the fiber, but the supercontinuum continued to broaden up to a length of 20 cm. Beyond this length, the supercontinuum spectral distribution remained similar indicating that nonlinear intensity dependent effects such as self-phase modulation and Raman self-frequency shift are negligible beyond 20 cm.

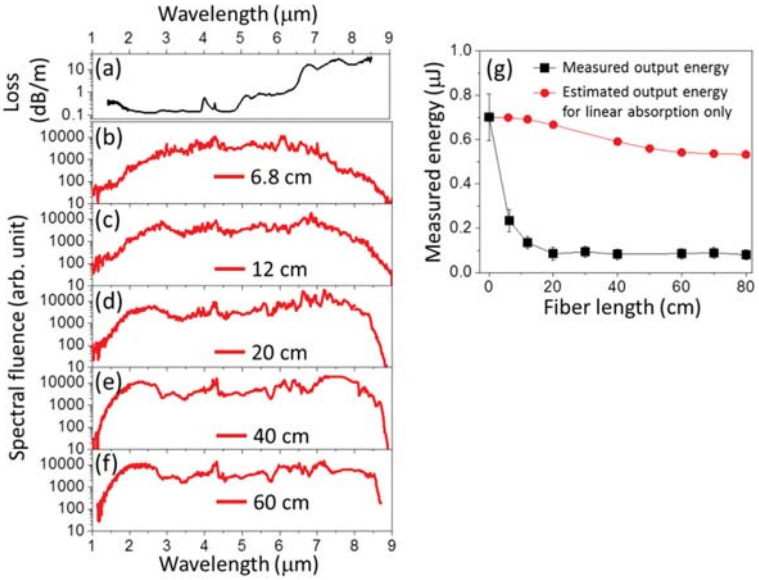

Fig. 5. (a) Transmission loss for the 100 µm core As_2S_3 fiber. (b)-(f) Spectral distribution of generated supercontinua for a injected MIR laser pulse centered at 4.56 µm and 700 nJ input energy for different As_2S_3 fiber length. (g) Measured output energy (black square) and estimated output energy based on measured supercontinuum spectral distribution and fiber linear absorption (red circle).

For 6.8 cm long fiber, the 10 dB spectral flatness of the supercontinuum already span from 2.0 µm up to 7.5 µm, while for the 20 cm long fiber, the 10 dB spectral flatness range from 1.7 µm up to 8.4 µm. Such spectral distribution is one of the broadest supercontinuum generated in large core As_2S_3 fibers [13–15]. It is also noteworthy that the supercontinuum distributions measured in Figs. 5(c)-5(f) present spectral dips at wavelengths between 3 µm and ~5.5 µm, which could result from the MIR NLA from the excited states in the As_2S_3 Urbach extension.

Figure 5(g) presents the overall transmitted infrared energy for different fiber lengths by using the cut-back technique. The detector used to measure the output energy is a Gentec THZ5I-BL-BNC broadband pyroelectric sensor having a constant spectral response between 1 µm and 10 µm. The energy injected into the fiber core was 700 nJ which corresponds to an input intensity around 70 GW/cm^2. The measured fiber output energy (black square in Fig. 5(g)) decreases quickly from 700 nJ to 100 nJ (decrease of 85%) as the fiber length increases up to 20 cm. Beyond 20 cm, the output energy remains almost constant, indicating here also

that the dispersion broadened the pulsewidth and the laser pulse intensity is sufficiently low to neglect the NLA.

Based on the measured spectral distribution of the generated supercontinuum for different fiber lengths (Figs. 5(b)-5(f)) and the linear loss of the fiber (Fig. 5(a)), we estimated the output energy if the loss was only due by the linear absorption of the fiber (red circle in Fig. 5(g)). This estimation points out that the energy loss due to the linear absorption is only 5% in the first 20 cm of the fiber, which is 17 times too low to explain the measured 100 nJ output energy at 20 cm long fiber. Therefore, in this case where high intensity 70 GW/cm^2 MIR pump pulse was injected into the core of the fiber, most of the energy loss are due to the NLA. It is interesting to note that by considering the fiber dispersion, the measured output energies and spectral distributions as a function of the fiber length, it was possible to extract similar NLA than the z-scan experiments performed in previous sections.

5. Summary

In conclusion, depending of the input laser intensity, the MIR NLA observed in As_2S_3 can be many orders of magnitude higher than its linear absorption. The observed NLA is due to two-photon excitation of valence electron to the Urbach extension followed by strong linear absorption of excited states. For most reported works on supercontinuum generation in As_2S_3 fiber [1–6], the MIR NLA might not be the main factor that limited the spectral broadening to 4-4.2 μm, especially when the S-H absorption band was very important. However, depending of the input laser parameters, the fiber core diameter and the fiber length used for the supercontinuum generation, the MIR NLA can affect significantly the efficiency and shape of the supercontinuum output spectra as demonstrated in Fig. 5. The impact of the NLA varies depending of the injected pump pulse wavelength and intensity. As an example, a MIR soliton of 1 kW peak power propagating in an As_2S_3 fiber having an effective mode diameter of 9 μm will experience a nonlinear loss of ~0.1 dB/m, which is similar to the background loss for most As_2S_3 fibers. For higher laser peak intensity, the MIR NLA increase very abruptly and can induce higher lost than the linear absorption in the spectral range between 3 μm and ~5 μm. Therefore, in order to optimize both the spectral bandwidth and the output power during supercontinuum generation in As_2S_3 fibers [13], it is important to maintain the MIR pump laser below a certain range of intensities inside the chalcogenide fiber core in order to avoid important NLA.

Acknowledgments

This work was supported by a Defence Research & Development Canada (DRDC) Program. The authors acknowledge technical support from Antoine Laramée and Hélène Gagnon. The authors also acknowledge the transmission loss measurement of the As_2S_3 fibers done by Christophe Lafond and Stéphane Châtigny from CorActive.